Electroreduction of CO 2 on Single-Site Copper-Nitrogen-Doped Carbon Material: Selective Formation of Ethanol and Reversible Restructuration of the Metal Sites

Dilan Karapinar, Ngoc Tran Huan, Nastaran Ranjbar sahraie, Jingkun Li, David Wakerley, Nadia Touati, Sandrine Zanna, Dario Taverna, Henrique Galvão Tizei, Andrea Zitolo, et al.

HAL Id: hal-02301443
https://hal.sorbonne-universite.fr/hal-02301443

Submitted on 30 Sep 2019

WILEY-VCH

Electroreduction of CO₂ on Single-Site Copper-Nitrogen-Doped Carbon Material: Selective Formation of Ethanol and Reversible Restructuration of the Metal Sites

Dilan Karapinar,[a] Ngoc Tran Huan, [a] Nastaran Ranjbar Sahraie,[b] Jingkun Li,[b] David Wakerley[a], Nadia Touati,[c] Sandrine Zanna,[c] Dario Taverna,[d] Luiz Henrique Galvão Tizei,[e] Andrea Zitolo,[f] Frédéric Jaouen,[b] Victor Mougel,[a],[g]* Marc Fontecave[a]*

Abstract: It is generally believed that CO_2 electroreduction to multi-carbon products such as ethanol or ethylene may be catalyzed with significant yield only on metallic copper surfaces, implying large ensembles of copper atoms. Here, we report on an inexpensive Cu-N-C material prepared *via* a simple pyrolytic route that exclusively feature single copper atoms with a CuN_4 coordination environment, atomically dispersed in a nitrogen-doped conductive carbon matrix. This material achieves aqueous CO_2 electroreduction to ethanol at a Faradaic yield of 55% under optimized conditions (electrolyte: 0.1 M $CsHCO_3$, potential: -1.2V *vs.* RHE and gas-phase recycling set up), as well as CO electroreduction to C_2-products (ethanol and ethylene) with a Faradaic yield of 80%. During electrolysis the isolated sites transiently convert into metallic copper nanoparticles, as shown by *operando* XAS analysis, which are likely to be the catalytically active species. Remarkably, this process is reversible and the initial material is recovered intact after electrolysis.

Introduction

The conversion of CO_2 to multi-carbon products is currently one of the most promising approaches to valorize CO_2 as fuels or chemical feedstocks. This may be achieved in electrolyzers *via* the electrochemical CO_2 reduction reaction (CO_2RR), providing the opportunity to store renewable but intermittent electric energy (sun, wind) as chemical fuels or other high-added-value products. Copper-based materials were early identified as catalysts that efficiently promote CO_2RR in aqueous conditions to C_2-products such as ethylene and ethanol [1]. Recent years have witnessed numerous studies on such electrode materials, reaching Faradaic yields (FY) for multi-carbon products as high as 60% [2]. Alcohols are desirable CO_2RR products, in particular ethanol, owing to their high energy-densities and ease of separation from the unreacted CO_2 gas stream. However, catalysts promoting alcohol production with high selectivity are still extremely rare.[2e-k, 3] Strategies to increase the selectivity of metallic-copper surfaces towards multi-carbon products are emerging through tailoring the surface properties of copper electrodes, either using a second metal [2k, 4], by controlled oxidation [2g, 5] or nanostructuration [6]. Alternatively, single-site catalysts have shown high CO_2RR activity and selectivity, however only afford single-carbon compounds, such as CO, methane or methanol as major products.[7]

Herein, we disclose the synthesis, characterisation and CO_2RR activity of a copper-nitrogen co-doped carbon material (Cu-N-C) presenting well-defined isolated CuN_4 sites covalently integrated into an amorphous carbon matrix (Fig. 1a). This material shows high selectivity for ethanol production in aqueous conditions, with a FY up to 55%. We demonstrate that ethanol is the sole liquid-phase product of CO_2RR and that CO is a key reaction intermediate in this process, as evidenced by the ability of the material to catalyse the electroreduction of CO to ethanol with a FY over 65%. In addition, while *ex-situ* characterization of the material after electrolysis shows a structure identical to the starting material with only isolated CuN_4 sites, o*perando* X-ray absorption (XAS) results clearly evidenced a restructuring of the material under electrocatalytic conditions, via partial and transient conversion of CuN_4 sites into Cu nanoparticles. Indeed, this is reversible since the latter convert back to CuN_4 sites after electrolysis.
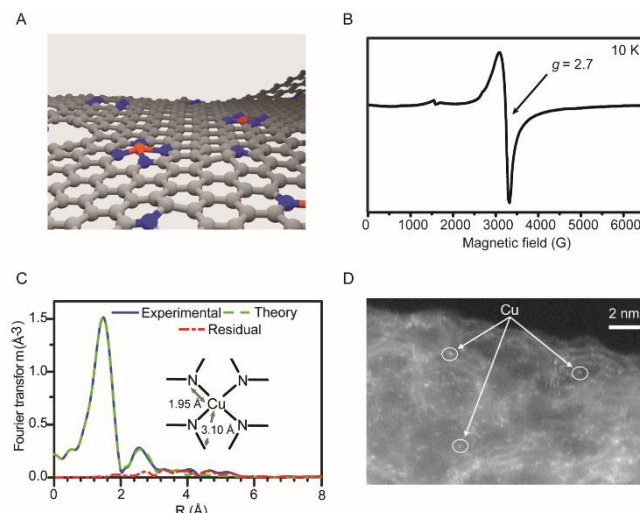
Results and Discussion

Synthesis and characterization of the Cu-N-C single-site material

[a]   D. Karapinar, Dr. N. T. Huan, Dr D. Wakerley, Prof. Dr. V. Mougel, Prof. Dr. M. Fontecave
        Laboratoire de Chimie des Processus Biologiques, CNRS UMR 8229
        Collège de France, Sorbonne Université, PSL Research University, 11 Place Marcelin Berthelot, 75231 Paris Cedex 05, France.
        Correspondence to: mougel@inorg.chem.ethz.ch;
        marc.fontecave@college-de-france.fr
[b]   Dr. N. Ranjbar Sahraie, Dr. J. Li, Dr. F. Jaouen
        Institut Charles Gerhardt Montpellier (UMR 5253), CNRS, Université de Montpellier
        ENSCM, 2 place Eugène Bataillon, 34095 Montpellier, France.
[c]   Dr. N Touati, Dr. S. Zanna
        Chimie ParisTech, PSL Research University, CNRS, Institut de Recherche de Chimie Paris (IRCP)
        11 rue Pierre et Marie Curie, 75005 Paris, France.
[d]   Dr. D. Taverna
        Institut de Minéralogie et de Physique des Milieux Condensés, UMR 7590 CNRS, Sorbonne Universités, UPMC Univ Paris 06
        4 place Jussieu, 75005 Paris, France.
[e]   Dr. L. H. Galvão Tizei
        Laboratoire de Physique des Solides
        Université Paris Sud, Bât 510, 91405 Orsay, France.
[f]   Dr. A. Zitolo
        Synchrotron SOLEIL
        L'Orme des Merisiers Saint-Aubin - BP 48, 91192 Gif-sur-Yvette, France.
[g]   Current address: Department of Chemistry and Applied Biosciences, ETH Zürich, Vladimir-Prelog-Weg 1-5, CH-8093 Zürich, Switzerland.

        Supporting information for this article is given via a link at the end of the document.

Pyrolytic synthesis has been identified as an effective route to produce atomically-dispersed metal ions coordinated to nitrogen atoms within carbon matrices [8]. By analogy to the synthetic routes developed for Fe-N-C materials used in O_2 electroreduction and CO_2RR,[7e, 8a] we successfully synthesized a single-site Cu-N-C material *via* a two-step strategy: (i) dry-phase mixing of a Zn based zeolitic imidazolate framework (ZIF-8) with Cu(II) chloride and phenanthroline ligand *via* low-energy ball-milling; (ii) pyrolysis of the resulting catalyst precursor powder at 1050 °C under Ar flow. We prepared the material **Cu$_{0.5}$NC**, comprising 0.5%$_{wt}$ Cu at step (i), which resulted in 1.4%$_{wt}$ Cu after pyrolysis as determined by elemental analysis (the increase in Cu %$_{wt}$ is due to ZIF-8 forming volatile products). A very small amount (< 0.02%$_{wt}$) of Zn, derived from ZIF-8, was also present as determined by Inductively Coupled Plasma – Atomic Emission Spectroscopy (ICP-AES). X-ray photoelectron spectroscopy (XPS) of **Cu$_{0.5}$NC** showed Cu 2p$_{3/2}$ peaks at 932.5 and 935.0 eV and a Cu-Auger line with a maximum at 569.0 eV (Figure S1), indicating +II is the predominant Cu oxidation state. The analysis of the N 1s region revealed the presence of pyridinic (398.6 eV), pyrrolic (401.0 eV), graphitic (402.6 eV) and porphyrin-like N-Cu signals (399.7 eV), analogous to that which is typically observed with Metal-N-C materials (Figure S1) [7e, 7f]. The presence of Zn was also confirmed by XPS analysis (Figure S1). At 10 K **Cu$_{0.5}$NC** displayed a continuous-wave electron paramagnetic resonance (EPR) spectrum with a broad signal centered at g = 2.07, typical for a Cu^{2+}, d^9 S=1/2 state (Figure 1b). Hyperfine coupling was not observed, probably due to the exchange interaction within the graphitic sheets. The threshold energy of the Cu K-edge X-ray absorption near-edge structure (XANES) spectrum of **Cu$_{0.5}$NC** is 8983.8 eV, similar to that of a Cu(II)-phthalocyanine molecular analogue (8984.6 eV). This further supports a predominant +II oxidation state of the Cu centers (Figure S2-S4). The Cu K-edge extended X-ray absorption fine structure (EXAFS) analysis of **Cu$_{0.5}$NC** is shown in Figure 1c and Figure S5. Fitting this spectrum with Cu-N and Cu-C scattering paths from the nearest neighbors reveals the presence of four N atoms at 1.95(1) Å from the Cu center, in agreement with values determined by EXAFS on copper-porphyrin [9]. The CuN$_4$ sites are integrated in the graphitic matrix, as revealed by the need for two shells of Cu-C scattering path at 3.10(2) and 3.36(2) Å (See Table S1) to properly fit the EXAFS spectrum. In addition, the absence of intense peaks at *ca.* 2.3 Å in the Fourier-transformed spectrum (Figure S6), characteristic for Cu-Cu scattering paths, suggests the absence of copper clusters. The absence of crystalline copper in our material was further confirmed by (i), powder X-ray diffraction of the material (Figure S7), revealing only two broad reflection peaks typical for nano-sized graphitic platelets in amorphous carbon materials [7e] and (ii), transmission electron microscopy (TEM) images showing amorphous carbon structures and no copper clusters (Figure S8). To gain deeper insight into the copper dispersion, atomic-resolution high-angle annular dark-field scanning transmission electron microscopy (HAADF-STEM) images of **Cu$_{0.5}$NC** were captured. These images (Figure 1d and Figure

Figure 1. Structural and morphological characterization of Cu$_{0.5}$NC. (a) Schematic representation; **(b)** EPR spectrum recorded at 10 K of **Cu$_{0.5}$NC** diluted in an amorphous silica matrix; **(c)** Cu K-edge EXAFS analysis in the Fourier-transformed space; **(d)** HAADF-STEM image.

S9) show the presence of multiple bright dots of atomic size, corresponding to isolated Cu atoms, as confirmed by electron energy loss spectroscopy at these sites (Figure S9b).

CO$_2$ electrocatalytic reduction

Cu$_{0.5}$NC was then evaluated for electrocatalytic CO$_2$ reduction after deposition on a carbon-based gas-diffusion layer (GDL) with a Nafion® perfluorinated resin binder. The latter served to stabilize the deposit but had no effect on the activity. The deposit did not significantly alter the morphology of the GDL layer, as shown by scanning electron microscopy (Figure S10). The electrode was initially investigated by controlled-potential electrolysis (CPE) at potentials ranging from –0.5 to –1.0 V (all potentials are indicated *vs.* RHE) under standard 'static headspace' conditions, *i.e.* in a closed cell, under a CO$_2$ atmosphere, containing CO$_2$-saturated 0.1 M aqueous solutions of various alkali bicarbonates (Li, Na, K, Cs). Linear sweep voltammograms (LSVs), CO production rates and current variation during electrolysis are reported in Figure S11-S16. As shown in Figure 2a and 2b, CO and H$_2$ were identified as the major reaction products, with the FY for CO, FY(CO), reaching a maximum at different potentials depending on the electrolyte (47 % at –0.8 V for LiHCO$_3$, 58 % at –0.7 V for NaHCO$_3$, 64 % at –0.6 V for KHCO$_3$ and 74 % at –0.6 V for CsHCO$_3$). The maximum FY(CO) increased with increasing the size of the cation in the order Li$^+$<Na$^+$<K$^+$<Cs$^+$. While this had been previously observed with metallic electrodes (Au, Ag, Cu, Hg),[10] it had not yet been reported for Metal-N$_4$-based or other carbon-supported catalysts. FY(H$_2$) increased at the expense of FY(CO) upon scanning towards more cathodic potentials. This can be

explained by considering the mass transport of the reactants. Indeed, the CO_2 concentration at the electrode surface decreases drastically with increasing current densities due to CO_2 consumption and stronger gas evolution from the electrode (which sparges the solution from CO_2) and as such protons become the dominant substrate due to their higher concentration in the bulk and higher diffusion coefficient. In this respect, the $CsHCO_3$ electrolyte is clearly unique since H_2 production did not significantly increase below –0.7 V. Such an effect has been attributed to the stronger cation hydration of Cs^+, reducing the cation-specific adsorption on the cathode and limiting H_2 production.[11] Additionally we observed a total FY for all gas-phase products well below 100% at electrode potentials below –0.9 V, indicating the formation of liquid phase products, in particular trace amounts of ethanol (Figure S12b). The very limited amount of CO_2 in CO_2-saturated aqueous solution under static CO_2 atmosphere together with a degassing of the electrolyte due to the formation of gaseous products at such negative potentials however greatly restrict the formation of more complex multi-carbon products . This led us to modify the operating conditions in a second step of the investigation. Indeed, to prevent CO_2 depletion during electrolysis and reach higher FY for such multi-carbon products, we thus carried out the catalytic tests under 'flow' conditions, providing a constant CO_2 supply to the electrolyte (10 mL/min), in 0.1 M $CsHCO_3$ as the electrolyte.
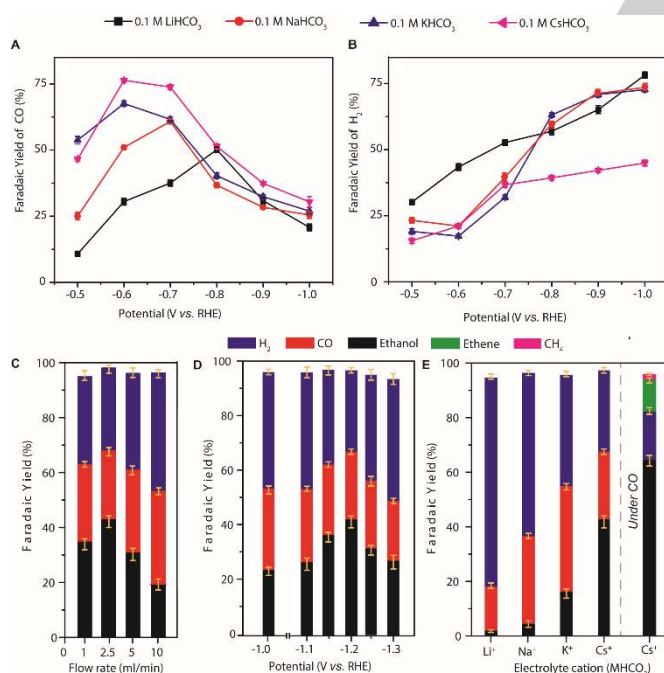

Figure 2. Faradaic yields of CO_2RR on $Cu_{0.5}NC$. Faradaic yields of (**a**) CO and (**b**) H_2 under 'static headspace' conditions after 10 minutes of CPE, in 0.1 M CO_2-saturated aqueous solutions of various alkali bicarbonates. FYs for CO_2RR under 'flow' conditions after 1 h of CPE: (**c**) at –1.2 V *vs*. RHE in a 0.1 M $CsHCO_3$ aqueous solution under various flow rates of CO_2. (**d**) at 2.5 mL/min CO_2 flow-rate in 0.1 M $CsHCO_3$ aqueous solution, at various applied potentials during CPE. (**e**) at –1.2 V *vs*. RHE and 2.5 mL/min flow rate of CO_2 in 0.1 M aqueous solutions using various electrolyte cations. FYs of CO reduction products after 1 h CPE at –1.2 V *vs*. RHE under 2.5 mL/min flow of CO in 0.1 M $CsHCO_3$ are reported on the right-hand side of Figure 2 (**e**).

CPE was carried out during one hour at potentials ranging from –1.0 V to –1.3 V, analyzing the gaseous products by on-line gas chromatography and the liquid phase products by quantitative ^{1}H NMR and ionic chromatography. Remarkably, ethanol was the sole product found in liquid phase at these potentials, while H_2 and CO were the only detected gas-phase products (Figure S17-S18).[12] The highest FY(EtOH) was obtained at –1.2 V (Figure S19). We further optimized the system by investigating the effect of CO_2 flow-rate on the ethanol production, while keeping the potential fixed at –1.2 V. A maximum FY(EtOH) of 43 % was found for a flow rate of 2.5 mL/min with a high and stable average current density of 16.2 mA/cm^2 (Figure 2c, Figure S20 and Table S2). At this optimized flow rate, the FY(EtOH) increased at all the potentials between –1.0 V and –1.3 V with respect to the catalytic test carried out at 10 mL/min flow rate, but the optimal potential remained at –1.2 V (Figure 2d). It should be noted that the FY for CO and H_2 did not vary during the electrolysis (Figure S18). As a reference material, the parent copper-free nitrogen-doped carbon material prepared identically, except for the absence of copper chloride in the precursor mixture, did not show any ethanol production (Figure S21). This demonstrated that the Zn atoms are not active in ethanol production. Whether such a low amount of Zn present on the material could nevertheless combine with Cu to provide the observed selectivity seems unlikely. Indeed, recent ZnCu alloys were reported to catalyze the electroreduction of CO_2, however exclusively into a mixture of CO and H_2 with no ethanol production[13] and Cu_xZn oxide catalysts were shown to produce ethanol, in addition to CO and H_2, however with an important co-production of ethylene.[2e]

To confirm that CO_2 constituted the carbon source for ethanol, we carried out the catalytic test using ^{13}C labeled CO_2 (–1.2 V, 2.5 mL/min CO_2). The ^{1}H and ^{13}C NMR of the liquid phase after 1h electrolysis revealed the quantitative ^{13}C labeling of ethanol (Figure S22-S23), validating that ethanol originates from CO_2 reduction. Finally, under optimized conditions (–1.2 V, 2.5 mL/min CO_2, Figure 2e) the larger cations again favored ethanol production with FY(EtOH) increasing in the order Li^+ (2%) < Na^+ (5%) < K^+(16%) < Cs^+ (43%).

As for many CO_2 reduction catalysts, the Tafel plot for $Cu_{0.5}NC$ is complex and the Tafel slope is strongly potential-dependent. We hence expressed the Tafel slopes resulting from the specific partial current densities of the different products. A Tafel slope of 175 mV/decade could be measured between –0.4 and –0.6 V applied potential for CO, as derived from "static headspace" experiments and a Tafel slope of 311 mV/decade for EtOH was estimated from "flow" experiments between –1.1 and –1.2 V applied potential (Figure S24). These different values suggest that the two reactions have different rate determining steps. In addition, the Tafel slope measured for ethanol is significantly higher than the slope of 120 mV/decade typically observed when the rate-determining step is a reductive coupling of adsorbed CO intermediates on metallic electrodes.[6d] Relatively large overpotential at 1 mA/cm^2 of 1 V was determined by Tafel-slope analysis of the partial current for ethanol. This value is in the range of the overpotentials observed with Cu foil in similar

reaction conditions[2a] but our catalyst shows a much narrower product distribution.

Assuming that CO is the most probable first reaction intermediate in the ethanol formation mechanism, we reasoned that the lower selectivity of **Cu0.5NC** for ethanol production at high CO_2 flow-rates could be explained by a decrease of local CO concentration at the electrode surface caused by the increased sparging. We hence carried out CPE using **Cu0.5NC** in 0.1 M $CsHCO_3$ aqueous solution at −1.2 V for 1 hour with a continuous 2.5 mL/min flow of CO (Figure S25). A stable current density of about 12 mA/cm² was observed and a FY(EtOH) of 66% was obtained , confirming that higher FY(EtOH) could be obtained if the CO concentration was increased (Figure 2e). Minor amounts of ethylene and methane were also observed.

This high FY for CO reduction to ethanol encouraged us to explore the recycling of the gas phase during CO_2RR, as significant amounts of CO were formed and could be further converted to ethanol. We hence carried out CPE at −1.2 V for 1 hour using a closed CO_2 volume of 300 mL cycled through the electrolyzer at a flow of 2.5 mL/min (Figure S26). In this setup the FY(EtOH) increased to 55%, with a concomitant decrease of FY for CO, in agreement with the favored reduction of CO to ethanol. In these conditions, methane was also identified as a minor product (Figure S27).

Ex-situ and *operando* characterization of the material

Ex-situ characterization of **Cu0.5NC** after electrolysis did not show any evidence for the presence of metallic copper nanoparticles: (i) no Cu nanoparticles could be observed in TEM images (Figure S28); (ii) no Cu^0 signal was detected in the XPS spectrum (Figure S29) and the XANES spectrum (Figure S30) either; (iii) no characteristic Cu-Cu feature from metallic copper or copper oxides could be observed in the Fourier Transform (FT) of the EXAFS spectrum which revealed that the material only contained CuN_4 sites before and after electrolysis (Figure S31). However, the *ex-situ* observation of isolated CuN_4 moieties may not be sufficient to conclude that these are the catalytic sites *per se.* In particular, recent studies of molecular Cu-phtalocyanine catalysts showed that very small metallic Cu nanoparticles formed *in-situ* during CO_2 electrolysis, however in a reversible way [14]. Whether such a behavior also occurs in the case of the CuN_4 sites of **Cu0.5NC** was studied by XAS in *operando* electrolysis conditions (Figure S32). Analysis of the XANES spectra at the copper K-edge of the material under electrocatalytic conditions revealed a shift in the edge position from 8983.93eV to 8979.2 eV for applied potentials below −0.6 V *vs.* RHE, indicative of a change of the Cu oxidation state from +II to 0 (the metallic copper K-edge energy position is indeed 8979 eV, see Figures 3, S3-S4). Consistently, Cu K-edge FT-EXAFS spectra of **Cu0.5NC** recorded under operating conditions demonstrated the appearance of a Cu-Cu coordination, showing that metallic copper nanoparticles extensively form under electrocatalytic conditions, even when moderate potentials (from −0.6 V *vs.* RHE) were applied.

In agreement with XANES data, the FT-EXAFS spectrum thus clearly indicated that Cu was essentially in the form of nanoparticles after prolonged electrolysis at −1.2 V *vs.* RHE (green spectrum Figure 3d), even though a very small peak at

around 1.5 Å was indicative of Cu atoms coordinated with light atoms (C, N, O). It is thus very likely that these nanoparticles are the catalytically active species. Nitrogen-doped carbon-supported Cu nanoparticles have been previously reported as highly active for the CO_2RR to ethanol.[15]

The mean size of these particles can be estimated by using EXAFS coordination numbers (CNs) and mean interatomic distances applying an equation valid for homogeneous spherical nanoclusters.[16] The details of the fitting procedure are provided in the experimental section. The best-fit analysis and the structural parameters obtained for Cu0.5NC at −1.2 V are reported in Figure S33 and Table S3, respectively, and compared to the crystalline Cu results. The estimated size of the Cu nanoparticles, by means of Cu-Cu first shell parameters, is 0.47±0.04 nm. While the coordination numbers obtained by the EXAFS analysis are probably underestimated, because a very small fraction of Cu is coordinated with light atoms, the experimental EXAFS spectrum can be correctly reproduced with Cu-Cu contributions only. The correction to be made to the CNs is small and affecting the particle size determination only marginally (*e.g.* for a system containing 20% of non-metallic Cu, which is a non-negligible fraction, the particle size estimation would be 0.53±0.05 nm).

Intrigued by the exclusive presence of CuN_4 sites in the *ex-situ* post electrolysis samples, we exposed the material used for the *operando* XAS measurements to air and, using XAS characterization, observed the disappearance of the metallic copper phase and the restoration of the original spectra (Figure 3 c-d). The same behavior occurred when the potential of the electrode was switched back to + 1 V *vs.* RHE, after electrolysis at −1.2 *vs.* RHE. This full structural reversibility operates upon multiple reduction/oxidation cycles. ICP measurement of Cu in the electrolyte upon cycling confirmed the absence of dissolved Cu, consistent with a quantitative binding of Cu in CuN_4 sites upon application of positive potentials. This is likely the consequence of the small size of the particles and the strong Cu(II)-chelating capacity of the N_4 sites of the material.
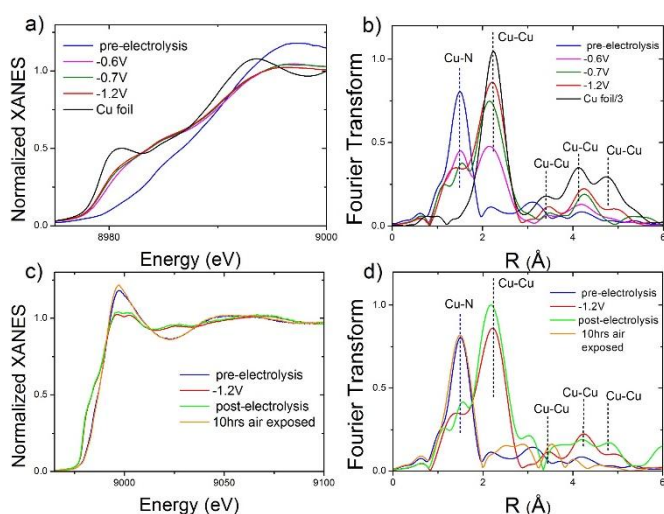
Figure 3. *Operando* XAS characterization of $Cu_{0.5}NC$ at the Cu-K edge. **(a)** K-edge XANES spectra of $Cu_{0.5}NC$ under no potential applied (blue line) ,$Cu_{0.5}NC$ during electrolysis at –0.6 V *vs.* RHE (pink line) , at –0.7 V *vs.* RHE (green line) , at –1.2 V *vs.* RHE (red line) and metallic copper (black line), **(b)** Fourier transform of the experimental EXAFS spectra of $Cu_{0.5}NC$ no potential applied (blue line) ,$Cu_{0.5}NC$ during electrolysis at –0.6 V *vs.* RHE (pink line) , at –0.7 V *vs.* RHE (green line) , at –1.2 V *vs.* RHE (red line) and metallic copper (black line), **(c)** Comparison between the K-edge XANES experimental spectrum of $Cu_{0.5}NC$ under no potential applied (blue line), $Cu_{0.5}NC$ during electrolysis at –1.2 V *vs.* RHE (red line), after electrolysis under no potential applied (green line) and $Cu_{0.5}NC$ after electrolysis at–1.2 V *vs.* RHE then sample exposed to air (orange line) **(d)** Fourier transform of the experimental EXAFS spectra of $Cu_{0.5}NC$ under no potential applied (blue line), $Cu_{0.5}NC$ during electrolysis at –1.2 V *vs.* RHE (red line), after electrolysis under no potential applied (green line) and $Cu_{0.5}NC$ after electrolysis at –1.2 V *vs.* RHE then sample exposed to air for 10 hours (orange line).

Conclusion

The novel material reported herein demonstrated the amenability of isolated copper CuN_4 sites as *precursors* for highly active catalysts for CO_2 electroreduction to ethanol. It is unique in allowing formation of ethanol as the *only* liquid product, reaching Faradaic yields as high as 55%. Optimization of the electrocatalytic conditions illustrated the importance of the electrolyte cation and the CO_2 flow-rate on the catalytic selectivity for EtOH formation. As shown in Table S4, these Faradic yields for ethanol are among the highest reported ones using Cu-based electrocatalysts. *Operando* XAS experiments established the conversion of the CuN_4 sites into very small metallic Cu nanoparticles during electrolysis. The latter are likely to be the catalytically active species, displaying a unique reactivity. Further studies of this material are required to understand the high selectivity observed. Interestingly, in the present case, the restructuring behavior is reversible which makes the material also a very stable catalyst. This study thus illustrates that extreme care must be taken before concluding on the nature of the active sites in such single-atom catalysts, even at very low metal loading. By demonstrating that the generation of multi-carbon products with high selectivity is possible using such site-isolated inexpensive material, this work paves the way towards new approaches to CO_2 electroreduction using single-site material precursors for improved selectivity and efficiency.

Acknowledgements

[1] Y. Hori, A. Murata, R. Takahashi, *Journal of the Chemical Society, Faraday Transactions 1: Physical Chemistry in Condensed Phases* **1989**, *85*, 2309-2326.

[2] a) K. P. Kuhl, E. R. Cave, D. N. Abram, T. F. Jaramillo, *Energy & Environmental Science* **2012**, *5*, 7050-7059; b) C. W. Li, M. W. Kanan, *Journal of the American Chemical Society* **2012**, *134*, 7231-7234; c) F. S. Roberts, K. P. Kuhl, A. Nilsson, *Angew. Chem.* **2015**, *127*, 5268-5271; d) H. Mistry, A. S. Varela, C. S. Bonifacio, I. Zegkinoglou, I. Sinev, Y.-W. Choi, K. Kisslinger, E. A. Stach, J. C. Yang, P. Strasser, B. R. Cuenya, *Nature Communications* **2016**, *7*, 12123; e) D. Ren, B. S.-H. Ang, B. S. Yeo, *ACS Catalysis* **2016**, *6*, 8239-8247; f) Y. Song, R. Peng, D. K. Hensley, P. V. Bonnesen, L. Liang, Z. Wu, H. M. Meyer, M. Chi, C. Ma, B. G. Sumpter, A. J. Rondinone, *ChemistrySelect* **2016**, *1*, 6055-6061; g) M. Rahaman, A. Dutta, A. Zanetti, P. Broekmann, *ACS Catalysis* **2017**, *7*, 7946-7956; h) K. Zhao, Y. Liu, X. Quan, S. Chen, H. Yu, *ACS Applied Materials & Interfaces* **2017**, *9*, 5302-5311; i) A. D. Handoko, K. W. Chan, B. S. Yeo, *ACS Energy Lett.* **2017**, *2*, 2103-2109; j) R. A. Geioushy, M. M. Khaled, K. Alhooshani, A. S. Hakeem, A. Rinaldi, *Electrochim. Acta* **2017**, *245*, 456-462; k) E. L. Clark, C. Hahn, T. F. Jaramillo, A. T. Bell, *Journal of the American Chemical Society* **2017**, *139*, 15848-15857.

[3] Y. Song, W. Chen, C. Zhao, S. Li, W. Wei, Y. Sun, *Angew. Chem. Int. Ed.* **2017**, *56*, 10840-10844.

[4] Y. Wang, D. Wang, C. J. Dares, S. L. Marquard, M. V. Sheridan, T. J. Meyer, *Proceedings of the National Academy of Sciences* **2018**, *115*, 278.

[5] a) K. W. Frese, *J. Electrochem. Soc.* **1991**, *138*, 3338-3344; b) M. Le, M. Ren, Z. Zhang, P. T. Sprunger, R. L. Kurtz, J. C. Flake, *Journal of The Electrochemical Society* **2011**, *158*, E45-E49; c) C. W. Li, J. Ciston, M. W. Kanan, *Nature* **2014**, *508*, 504; d) A. Dutta, M. Rahaman, N. C. Luedi, M. Mohos, P. Broekmann, *ACS Catalysis* **2016**, *6*, 3804-3814.

[6] a) W. Tang, A. A. Peterson, A. S. Varela, Z. P. Jovanov, L. Bech, W. J. Durand, S. Dahl, J. K. Norskov, I. Chorkendorff, *Phys. Chem. Chem. Phys.* **2012**, *14*, 76-81; b,9 D. Ren, N. T. Wong, A. D. Handoko, Y. Huang, B. S. Yeo, *The Journal of Physical Chemistry Letters* **2016**, *7*, 20-24; c) C. Reller, R. Krause, E. Volkova, B. Schmid, S. Neubauer, A. Rucki, M. Schuster, G. Schmid, *Advanced Energy Materials* **2017**, *7*, 1602114; d) D. Kim, C. S. Kley, Y. Li, P. Yang, *Proc. Nat. Acad. Sci.* **2017**, *114*, 10560-10565.

[7]   a) A. S. Varela, N. Ranjbar Sahraie, J. Steinberg, W. Ju, H.-S. Oh, P. Strasser, *Angewandte Chemie International Edition* **2015**, *54*, 10758-10762; b) P. Kumar, H. P. Mungse, O. P. Khatri, S. L. Jain, *RSC Advances* **2015**, *5*, 54929-54935; c) Z. Weng, J. Jiang, Y. Wu, Z. Wu, X. Guo, K. L. Materna, W. Liu, V. S. Batista, G. W. Brudvig, H. Wang, *Journal of the American Chemical Society* **2016**, *138*, 8076-8079; d) S. Kusama, T. Saito, H. Hashiba, A. Sakai, S. Yotsuhashi, *ACS Catalysis* **2017**, *7*, 8382-8385; e) T. N. Huan, N. Ranjbar, G. Rousse, M. Sougrati, A. Zitolo, V. Mougel, F. Jaouen, M. Fontecave, *ACS Catalysis* **2017**, *7*, 1520-1525; f) W. Ju, A. Bagger, G.-P. Hao, A. S. Varela, I. Sinev, V. Bon, B. Roldan Cuenya, S. Kaskel, J. Rossmeisl, P. Strasser, *Nature Communications* **2017**, *8*, 944; g) M. Gong, Z. Cao, W. Liu, E. M. Nichols, P. T. Smith, J. S. Derrick, Y.-S. Liu, J. Liu, X. Wen, C. J. Chang, *ACS Central Science* **2017**, *3*, 1032-1040; h) B. Reuillard, K. H. Ly, T. E. Rosser, M. F. Kuehnel, I. Zebger, E. Reisner, *Journal of the American Chemical Society* **2017**, *139*, 14425-14435; i) A. S. Varela, W. Ju, P. Strasser, *Advanced Energy Materials* **2018**, *8*, 1703614.

[8]   a) A. Zitolo, V. Goellner, V. Armel, M.-T. Sougrati, T. Mineva, L. Stievano, E. Fonda, F. Jaouen, *Nat. Mater.* **2015**, *14*, 937-942; b) H. T. Chung, D. A. Cullen, D. Higgins, B. T. Sneed, E. F. Holby, K. L. More, P. Zelenay, *Science* **2017**, *357*, 479.

[9]   F. Carrera, E. S. Marcos, P. J. Merkling, J. Chaboy, A. Muñoz-Páez, *Inorg. Chem.* **2004**, *43*, 6674-6683.

[10]   a) M. Akira, H. Yoshio, *Bull. Chem. Soc. Jpn.* **1991**, *64*, 123-127; b) M. R. Singh, Y. Kwon, Y. Lum, J. W. Ager, A. T. Bell, *Journal of the American Chemical Society* **2016**, *138*, 13006-13012; c) J. Resasco, L. D. Chen, E. Clark, C. Tsai, C. Hahn, T. F. Jaramillo, K.

Chan, A. T. Bell, *Journal of the American Chemical Society* **2017**, *139*, 11277-11287.

[11]   M. R. Thorson, K. I. Siil, P. J. A. Kenis, *Journal of The Electrochemical Society* **2013**, *160*, F69-F74.

[12]   Trace amount of acetate – below 3.5% FE – were observed when using $^{13}CO_2$ (Figure S23-S24). The $^{13}CO_2$ used in this study was analyzed and shown to contain significant amounts of O_2, CO and methane. Poisoning of some surface sites or undesired side-reaction with these impurities potentially explains the presence of this trace acetate by-product in the liquid phase.

[13]   a) P. Moreno-García, N. Schlegel, A. Zanetti, A. Cedeño López, M. d. J. Gálvez-Vázquez, A. Dutta, M. Rahaman, P. Broekmann, *ACS Applied Materials & Interfaces* **2018**, *10*, 31355-31365; b) S. Lamaison, D. Wakerley, D. Montero, G. Rousse, D. Taverna, D. Giaume, D. Mercier, J. Blanchard, H. N. Tran, M. Fontecave, V. Mougel, *ChemSusChem* **2019**, *12*, 511-517.

[14]   Z. Weng, Y. Wu, M. Wang, J. Jiang, K. Yang, S. Huo, X.-F. Wang, Q. Ma, G. W. Brudvig, V. S. Batista, Y. Liang, Z. Feng, H. Wang, *Nature Communications* **2018**, *9*, 415.

[15]   Y. Song, R. Peng, D. K. Hensley, P. V. Bonnesen, L. Liang, Z. Wu, H. M. Meyer III, M. Chi, C. Ma, B. G. Sumpter, A. J. Rondinone, *ChemistrySelect* **2016**, *1*, 6055-6061.

[16]   M. Borowski, *Journal De Physique Iv - J PHYS IV* **1997**, *7*.